atmosphere

MDPI

Article

Influence of the Atlantic Multidecadal Oscillation on South American Atmosphere Dynamics and Precipitation

Jelena Maksic [1,*], Marília H. Shimizu [2], Mary T. Kayano [2], Cristiano M. Chiessi [3], Matthias Prange [4] and Gilvan Sampaio [2]

[1] Division of Impacts, Adaptation and Vulnerabilities (DIIAV), National Institute for Space Research (INPE), Sao Jose dos Campos 12227-010, Brazil
[2] General Coordination of Earth Science (CGCT), National Institute for Space Research (INPE), Sao Jose dos Campos 12227-010, Brazil
[3] School of Arts, Sciences and Humanities, University of Sao Paulo, Sao Paulo 01156-000, Brazil
[4] MARUM—Center for Marine Environmental Sciences and Faculty of Geosciences, University of Bremen, 28359 Bremen, Germany
* Correspondence: jelena.maksic@inpe.br

Abstract: The Atlantic Multidecadal Oscillation (AMO) is coherently linked to climate variations over many parts of the globe. Despite recent achievements, the mechanism by which the AMO influences regional precipitation over South America is not well understood. In this study, we isolate the atmospheric response to the AMO using a water isotope-enabled version of the Community Earth System Model version 1.2 (iCESM1.2) and determine its influence on (sub)tropical South American regional precipitation and atmospheric circulation. The results suggest an interhemispheric seesaw in Hadley circulation strength and that the section of the Atlantic Hadley cell is marked by a stronger upward air component south of the equator during the cold AMO phase. We also find that the precipitation anomalies over (sub)tropical South America during AMO phases are mainly related to changes in the Atlantic Intertropical Convergence Zone (ITCZ) core strength, where in the cold (warm) AMO phase the core region strengthens (weakens) from February to July, while from July to November the core region weakens (strengthens). Our results stress the importance of acknowledging the dynamics of season- and regional-dependent ITCZ responses, as they are sufficient to produce observed AMO-related signals even in the absence of marked changes in the ITCZ position.

Keywords: AMO; ITCZ; iCESM1.2 model South America; isotope-enabled

Citation: Maksic, J.; Shimizu, M.H.; Kayano, M.T.; Chiessi, C.M.; Prange, M.; Sampaio, G. Influence of the Atlantic Multidecadal Oscillation on South American Atmosphere Dynamics and Precipitation. *Atmosphere* **2022**, *13*, 1778. https://doi.org/10.3390/atmos13111778

Academic Editors: Stefan Liess and Seon Tae Kim

Received: 28 July 2022
Accepted: 23 October 2022
Published: 28 October 2022

1. Introduction

The Atlantic Multidecadal Oscillation (AMO) is a pattern of variability in the North Atlantic sea surface temperature (SST), with alternations between warm and cold conditions in most of the basin, that was first identified during the 1980s [1]. There are a variety of methods for constructing the AMO index [2–6]. Although these indices consider different aspects of basin or sub-basin-scale variability, they all capture large-scale multidecadal SST anomalies: (i) an anomalously warm North Atlantic characterizes the warm AMO phase; and (ii) an anomalously cold North Atlantic characterizes the cold AMO phase. The warm and cold phases swing with a period of 60–90 years [7,8].

Regardless of the origins of the AMO, it is coherently linked to climate variations over many parts of the globe. It affects the Atlantic hurricane activity [9], North American and European summer climate [10], African Sahel rainfall [9,11], Asian monsoon [12–14], and summer rainfall over India [15]. Over South America, important linkages with the AMO have been described for precipitation variability over northeastern Brazil [8,16], surface air temperature of southern South America [17], and the dynamics of low-level jets [18,19]. More specifically, Jones and Carvalho [18] analyzed the influence of the AMO on decadal to multidecadal variability in the South American low-level jet (SALLJ). They

found a consistent pattern in which SALLJ days during cold AMO phases were associated with negative precipitation anomalies over northern Amazon and the Atlantic Intertropical Convergence Zone (ITCZ). The results indicate a stronger influence of the cold AMO during austral winter (May–September) than during austral summer (December–February), while in the exit region of the SALLJ over southern Brazil, Uruguay and northern Argentina, precipitation increases. Despite recent achievements, the mechanism by which the AMO influences regional precipitation over South America is not well understood. This is mostly due to the fact that observational data only contain two full cycles of the AMO.

By indirectly recording past precipitation changes, paleoclimate archives provide insights into the past behavior of the AMO. While there are records in which this multi-decadal climate variability is not a persistent feature before 1750 AD [20], an increasing number of records, summarized by Zhang et al. [21] indicate that the AMO variability extends several millennia back in time. Multiple archives from South America indicate that the AMO played a relevant role in modulating the South American Monsoon System (SAMS) during the last deglaciation [22] over the Holocene [23], and over the past 2000 years [24,25]. The prevailing view in the literature explains wet (dry) conditions in the SAMS domain by the southward (northward) shift of the Atlantic ITCZ and its influence on the SAMS and the South Atlantic Convergence Zone (SACZ) intensity. Both ITCZ and AMO are recognized to have strong imprints on the SAMS and the SACZ [26,27]. Due to shortness of the instrumental data and the scarcity of pre-instrumental proxy data reconstructions, insights must necessarily rely on analyses of climate models. However, despite the continuous improvement of climate models over the past two decades [28–30] coupled models still show a large spread on the anomalies in regional precipitation associated with the AMO [5,31–33].

In this study, we isolate the atmospheric response to the AMO using an Earth System model, and determine the influence of the AMO on (sub)tropical South American regional precipitation and atmospheric circulation. This simplified approach excludes the full range of feedbacks between different components of the climate system, as well as avoiding the introduction of biases related to the way the atmosphere is coupled to land or ocean, that are present in fully coupled models [34–38].

2. Materials and Methods

2.1. iCESM Model Setup

We carried out experiments with a water-isotope-enabled version of the Community Earth System Model version 1.2 (iCESM1.2). The iCESM1.2 has active atmosphere, land, ocean, river transport, and sea ice component models linked through a coupler, and also simulates global variations in water isotopic ratios in the atmosphere, land, ocean, and sea ice. For a detailed description of the model, validation and sensitivity analyses see [39,40]. In this study, we ran the atmospheric component of iCESM1.2, the isotope-enabled Community Atmosphere Model version 5 (iCAM5.3) [41], which is based on the original, non-isotope-enabled CAM5 [42], with prescribed SST and sea ice concentrations (SICs) coupled exclusively with an interactive land component, version 4 CLM4; [43]. The model was configured to use a computational grid of 1.9° latitude × 2.5° longitude and 30 vertical levels from the surface to ~3.5 hPa.

2.2. Experiments

The list of experiments performed with iCESM1.2, as well as the initialization procedure and the datasets for sea-ice concentrations and SST, can be found in Table 1. All experiments were initialized from pre-industrial conditions, where the values for greenhouse gasses, aerosols, ozone, and solar irradiance were fixed at the year 1850. Sea-ice concentrations (SIC) were taken from the Hadley Centre Global Sea Ice and Sea Surface Temperature (HadISST) dataset [44].

The CONTROL experiment is a 30-year-long simulation (with spin-up of 10 years) forced by climatological monthly mean SSTs from the HadISST.

Table 1. Description of the experiments performed with the water isotope-enabled version of the Community Earth System Model version 1 (iCESM1.2).

Experiment	Initialization	Sea-Surface Temperatures (SST) and Sea-Ice Concentrations (SIC)	Simulation
CONTROL	Pre-industrial conditions	HadISST dataset (Rayner et al., 2003)	One ensemble member/30 yr
CAMO	Pre-industrial conditions	Cold SST anomaly superimposed on the HadISST dataset (Rayner et al., 2003)	Three ensemble members/50 yr
WAMO	Pre-industrial conditions	Warm SST anomaly superimposed on the HadISST dataset (Rayner et al., 2003)	Three ensemble members/50 yr

The cold and warm AMO (CAMO and WAMO, respectively) experiments are an ensemble of three 50-year-long simulations (with 20 years of spin-up) produced by slight variations in initial atmospheric conditions. To isolate the atmospheric response to the AMO, we forced the model with the superimposed AMO-related anomalies onto the climatological monthly mean SSTs from the HadISST. The superimposed SST anomalies came from a composite analysis of the linearly detrended (1850–2012) HadSST2 dataset [44]) for each AMO phase. Following Trenberth and Shea (2006), the cold AMO phase included the 1850–1928 and 1964–1995 periods, and the warm AMO phase included the 1928–1964 and 1995–2012 periods. The use of the Trenberth and Shea (2006) AMO index isolates the Atlantic variability from global warming and tropical influences.

All results presented in the next sections refer to the ensemble mean and represent changes strictly forced by SST changes, as the two experiments only differ with respect to the prescribed SST/SIC in the North Atlantic region (Figure 1).

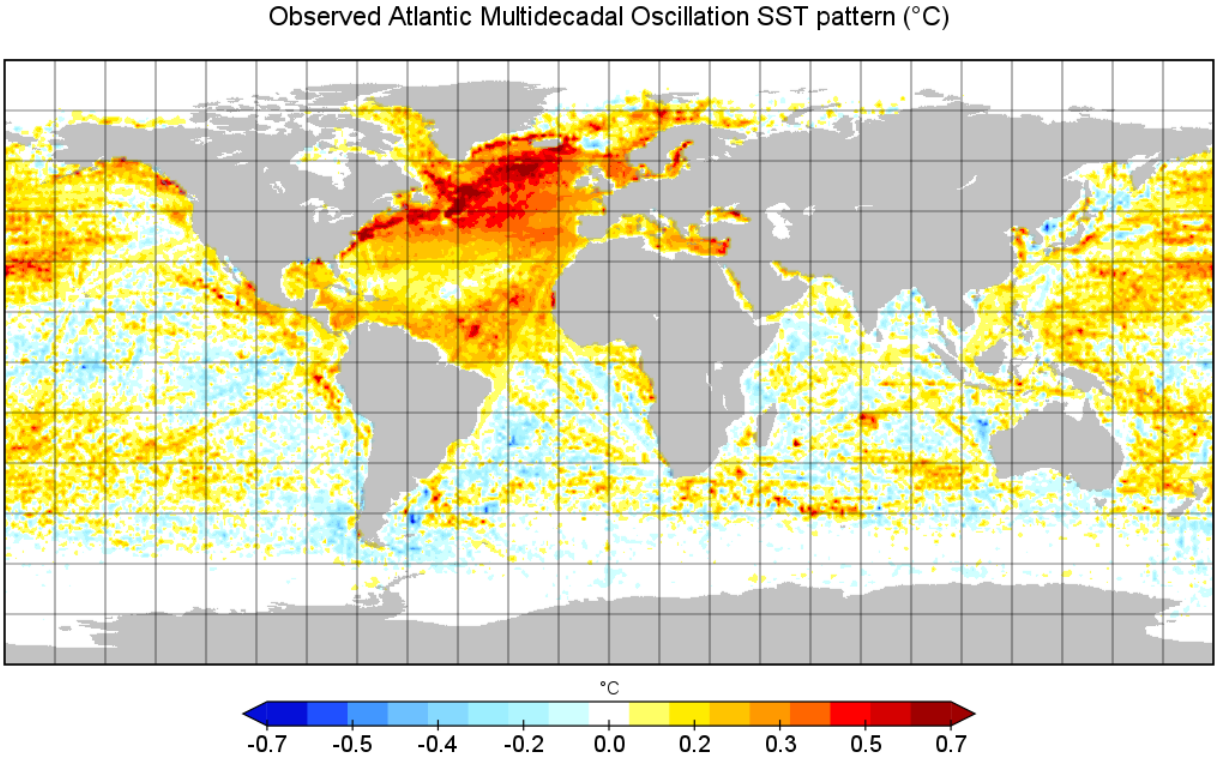

Figure 1. Computed annual sea surface temperature (SST) difference between the warm and cold Atlantic Multidecadal Oscillation (AMO) phases (°C). Phases are defined based on AMO index (Trenberth and Shea, 2006) using the HadISST dataset for the period 1870–2015.

2.3. Climate Variables and Methods Used in Analyses

The climate variables used to identify the main differences in CAMO and WAMO simulations include: precipitation, meridional and zonal winds, and vertical velocity. Thus, the effects of AMO-related SST over South American climate were evaluated through the differences between CAMO and WAMO experiments for precipitation (seasonal and annual mean), atmospheric circulation at 850 hPa (seasonal mean) and 200 hPa (austral summer mean), 200 hPa divergence (annual), and zonal and meridional vertical velocity profiles. The statistical significance of these differences was assessed using Student's *t*-tests at a 95% confidence level to evaluate whether the means of two different groups were distinct, meaning that the change was significant, or not. Student's *t* test is a hypothesis test for evaluating whether the means of two different groups (i.e., the CAMO and WAMO experiments versus the CONTROL experiment) are distinct, meaning that the change is significant, or not. In our case, the *t* value was calculated as follows:

$$t = \frac{M_E - M_C}{\sqrt{\frac{S_E^2}{nE} + \frac{S_C^2}{nC}}}$$

where M_E and M_C are the mean values, S_E and S_C are the standard deviations, and nE and nC are the number of samples. The subscripts E refer to the CAMO (WAMO) experiment and C refers to the CONTROL experiment. This t value is compared with the t value of the reference, which is dependent on the number of samples and level of confidence. The level of confidence means that our conclusion about the test, that is, whether the two groups are distinct or not, has a certainty of 95%.

Additionally, the upper-level divergence simulated by the CAMO and WAMO experiments were compared with those obtained from composite analyses for both AMO phases using data derived from the National Oceanic and Atmospheric Administration/Cooperative Institute for Research in Environmental Sciences/USA Department of Energy (NOAA/CIRES/DOE) third version of the 20th Century Reanalysis data (20CRv3) [45]. This comparison is important for detecting aspects of the AMO-driven upper-level convective changes captured in our simulations.

We also aimed to analyze the influence of the SSTs in both AMO phases on the atmospheric circulation cells. In our study, the meridional mean of vertical pressure velocity between 0° and 15° S represents the Walker cell, while the zonal mean of vertical pressure velocity between 80° W and 30° W represents the Hadley cell. The Hadley cell intensity changes between CAMO and WAMO experiments were calculated as the mean maximum value of the zonal-mean meridional stream function between 900 and 200 hPa [46].

Finally, as precipitation of South America is strongly influenced by changes in the ITCZ, and knowing that instrumental records suggest that AMO phases are actually coupled with ITCZ north–south migrations [47], we analyzed changes in ITCZ position through a zonal mean precipitation diagram.

3. Results

3.1. Changes in Precipitation

The spatial distributions of changes in precipitation between CAMO and WAMO are shown in Figure 2. The annual mean shows increased precipitation during the cold AMO phase, mainly in the Amazon and northeastern Brazil (Figure 2e). In contrast, the model simulates precipitation reduction in most northern regions of South America. Figure 2 also shows that the atmospheric response to the prescribed SST anomalies is seasonally dependent. During austral summer (December to February—DJF), the precipitation over most of South America is increased in the CAMO experiment, with significant differences in the western Amazon (0°–10° S, 55°–75° W), northeastern Brazil (1°–18° S, 35°–47° W) and the Andes (Figure 2a). In austral autumn (March to May—MAM), wetter conditions remain over the northeastern Amazon basin and in the northernmost portion of northeastern Brazil, while over most of South America, precipitation decreased (Figure 2b). On the other hand,

during the winter season (June to August—JJA) the model suggests significantly wetter conditions over most of northern and central-southern South America in CAMO and drier conditions in a small eastern sector of northeastern Brazil (Figure 2c). Wetter conditions over northeastern Brazil and almost the entire Andes and Amazonia, and drier conditions over southeastern South America occur during austral spring (September to November—SON) (Figure 2d). We also observe significant differences in the amount of precipitation over the Atlantic Ocean. There are significant differences in the amount of precipitation over the equatorial Atlantic Ocean for all seasons, with the largest increase occurring to the south of the equator close to northeastern Brazil, and the largest reduction to the north of the equator over the western and central Atlantic Ocean (Figure 2). Our simulated anomalies are comparable to reanalysis precipitation patterns (Figure S1), especially in most northern regions of South America and the tropical Atlantic (DJF, MAM). These anomalies are likely associated with changes in the Atlantic ITCZ, and further analyses on the ITCZ position and intensity are performed and presented later in this section. The simulated JJA and SON means are also in good agreement with reanalysis profiles, where the model reproduces the increase in precipitation in central South America.

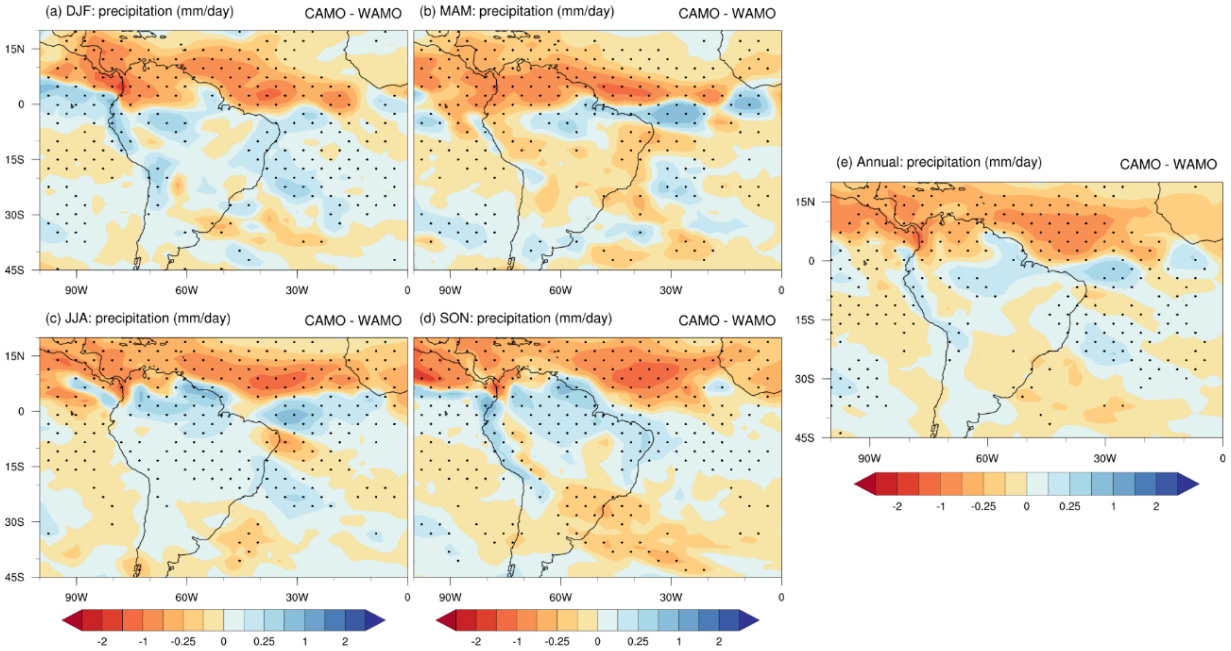

Figure 2. Seasonal precipitation differences between the cold Atlantic Multidecadal Oscillation (CAMO) and the warm Atlantic Multidecadal Oscillation (WAMO) experiments (mm/day) in (**a**) December–February (DJF), (**b**) March–May (MAM), (**c**) June–August (JJA), and (**d**) September–November (SON) and (**e**) annual mean. Red (blue) shaded areas correspond to drier (wetter) conditions; grid points with statistically significant difference according to Student's *t* test with confidence level of 95% are marked with dots.

To understand the dynamical mechanisms that caused the changes in precipitation, we analyzed the austral summer upper-level and lower-troposphere circulation (Figures 3 and 4). The position of the upper-level anticyclonic circulation, known as the Bolivian High, is the same for both CAMO and WAMO experiments, but the wind circulation is slightly intensified in WAMO (Figure 3b,c) in comparison with CAMO (Figure 3a,c) experiment, which enhanced the westerlies (200 hPa) over the North Atlantic Ocean, between the equator and 20N. Additionally, differences between CAMO and WAMO (Figure 3c) show that the subtropical jet stream is intensified in WAMO experiment, in relation to CAMO.

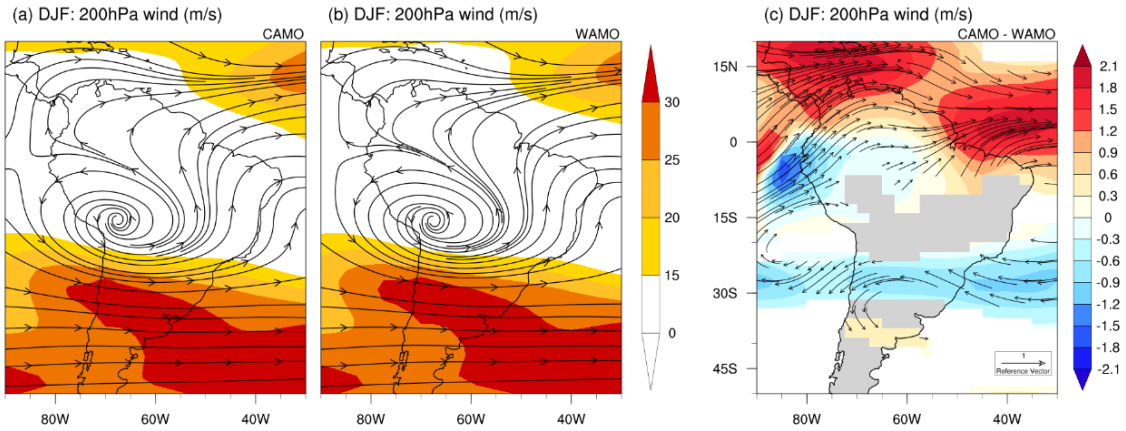

Figure 3. Streamlines and wind intensity (m/s) at 200 hPa for December–February (DJF) for the cold Atlantic Multidecadal Oscillation (CAMO) (**a**) and the warm Atlantic Multidecadal Oscillation (WAMO) (**b**) experiments, as well as for the differences between CAMO and WAMO (**c**). In (**c**), only statistically significant differences calculated using Student's *t* test with a confidence level of 95% are shown.

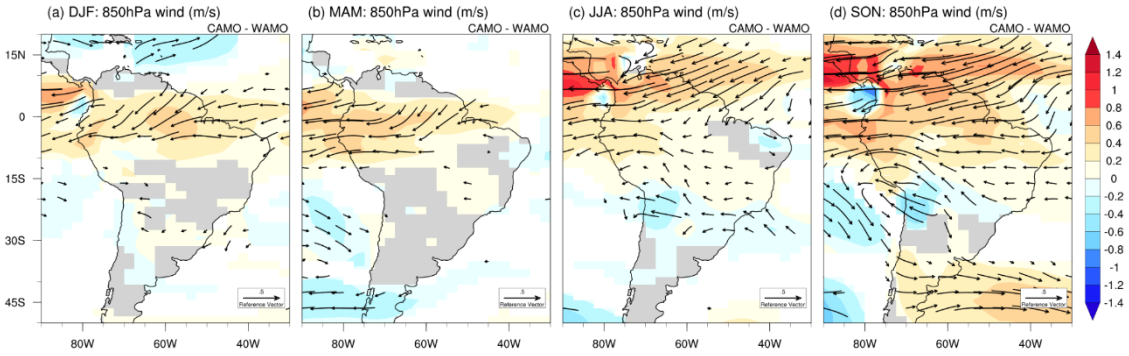

Figure 4. Seasonal wind vectors and intensity at 850 hPa (m/s) for the differences between the cold Atlantic Multidecadal Oscillation (CAMO) and the warm Atlantic Multidecadal Oscillation (WAMO) phases in (**a**) December–February (DJF), (**b**) March–May (MAM), (**c**) June–August (JJA), and (**d**) September–November (SON). Only statistically significant differences calculated using Student's *t* test with confidence level of 95% are shown.

Comparing the 850 hPa wind field anomalies between both AMO phases (Figure 4), an increased easterly flow reaching 10° S is noted for CAMO. A stronger low-level easterly flow, over most of the Amazon, brings more moisture to the mainland and correlates with the increase in precipitation over the Amazon and coastal northeastern Brazil. These anomalies are present in all months, but are stronger in JJA and SON (Figure 4c,d). There are also slightly stronger northerly low-level winds in the Chaco low region in SON (Figure 4d). The differences in the SALLJ are only significant in JJA and SON, and show a weakening in CAMO, reducing the moisture flow from the Amazon to southeastern South America.

As ascending vertical motion at upper levels (200 hPa) is associated with important elements of the SAMS such as SACZ, the Bolivian High circulation and northeastern Brazil, we compared the 200 hPa divergence fields for CAMO and WAMO and their differences with the 20CRv3 reanalysis data (Figure 5). The cold AMO phase is characterized by lower divergence over the Amazon and the equatorial North Atlantic and higher divergence over northeastern Brazil, in relation to the warm AMO phase (Figure 5a–c). Although the model has some deficiencies in representing the intensity of the upper-level convergence change between AMO phases in the Amazon, the simulated annual mean is in good agreement with reanalysis profiles, and the model reproduces the main features of the divergent circulation over South America, associated with both the ITCZ and the SACZ convection.

The differences between CAMO and WAMO show a dipole of lower/higher divergence over the tropical Atlantic, which is in agreement with the 20CRv3 data, and reflects the large SSTs anomalies over the region (Figure 1).

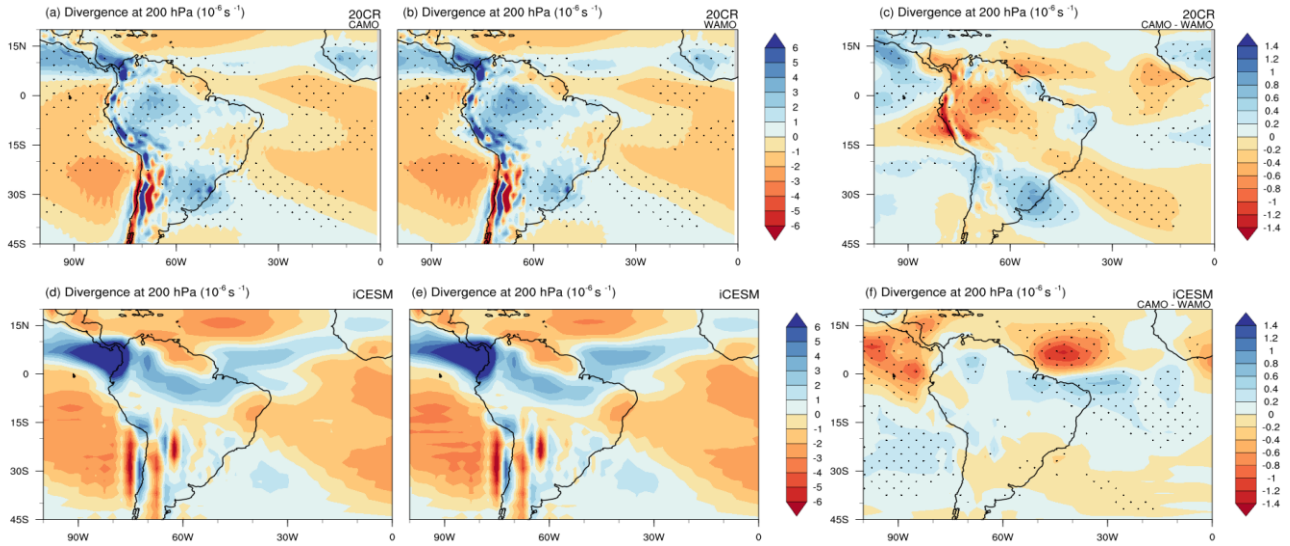

Figure 5. Divergence at 200 hPa for the cold Atlantic Multidecadal Oscillation (CAMO) and the warm Atlantic Multidecadal Oscillation (WAMO) phases, as well as the differences between both phases from reanalysis (**a**–**c**) 20CRv3 and (**d**–**f**) iCESM model. Stippling areas represent statistically significant (Student's *t* test at 95%) composites (**a**,**b**) and differences (**c**,**f**).

3.2. ITCZ and Atmospheric Circulation Cells

To identify changes in the Atlantic ITCZ, we analyzed the annual cycle of precipitation over the Atlantic (15° N–15° S) averaged over 40° W–0° for CAMO and WAMO (Figure 6a,c), and the differences between these experiments averaged over the whole longitudinal band (Figure 6b) and over 30° W, where the anomaly was the highest (Figure 6d). Although we cannot observe clear shifts in the mean position of the precipitation band (Figure 6a,c), distinct positive precipitation anomalies (CAMO-WAMO) are simulated from February to July between the equator and 10° S (highlighted by the blue rectangle on Figure 6b,d). It is worth noting the negative anomalies north and south of the positive anomaly field. We also found that precipitation weakens (intensifies) in the ITCZ core region during the CAMO (WAMO) after July (highlighted by the pink ellipse in Figure 6a,c), and their difference (highlighted by the pink rectangle in Figure 6b,d).

The zonal mean meridional stream function for both the CAMO and WAMO experiments (Figure 7) show negative and positive cells north and south of the equator, respectively, which represents the Northern and Southern Hemisphere (NH and SH) Hadley cells. In the intersection of these cells lies the ITCZ (black line near the equator), which is located a few degrees north of the equator in both experiments. Therefore, CAMO and WAMO experiments did not show substantial differences in the mean position of the Hadley cells and the ITCZ. However, the Hadley cell was stronger (weaker) in the NH (SH) for the CAMO experiment in relation to the WAMO experiment (Table 2).

Table 2. Mean intensity of the Northern Hemisphere (NH) and the Southern Hemisphere (HS) Hadley cells calculated in terms of vertical-mean (900–200 hPa) and zonal-mean meridional stream function ψ (10^9 kg/s) for CAMO and WAMO experiments, and the differences between them.

	CAMO (10^9 kg/s)	**WAMO (10^9 kg/s)**	**CAMO-WAMO (10^9 kg/s)**
NH	66.83	65.49	1.34
SH	−75.25	−78.23	2.98

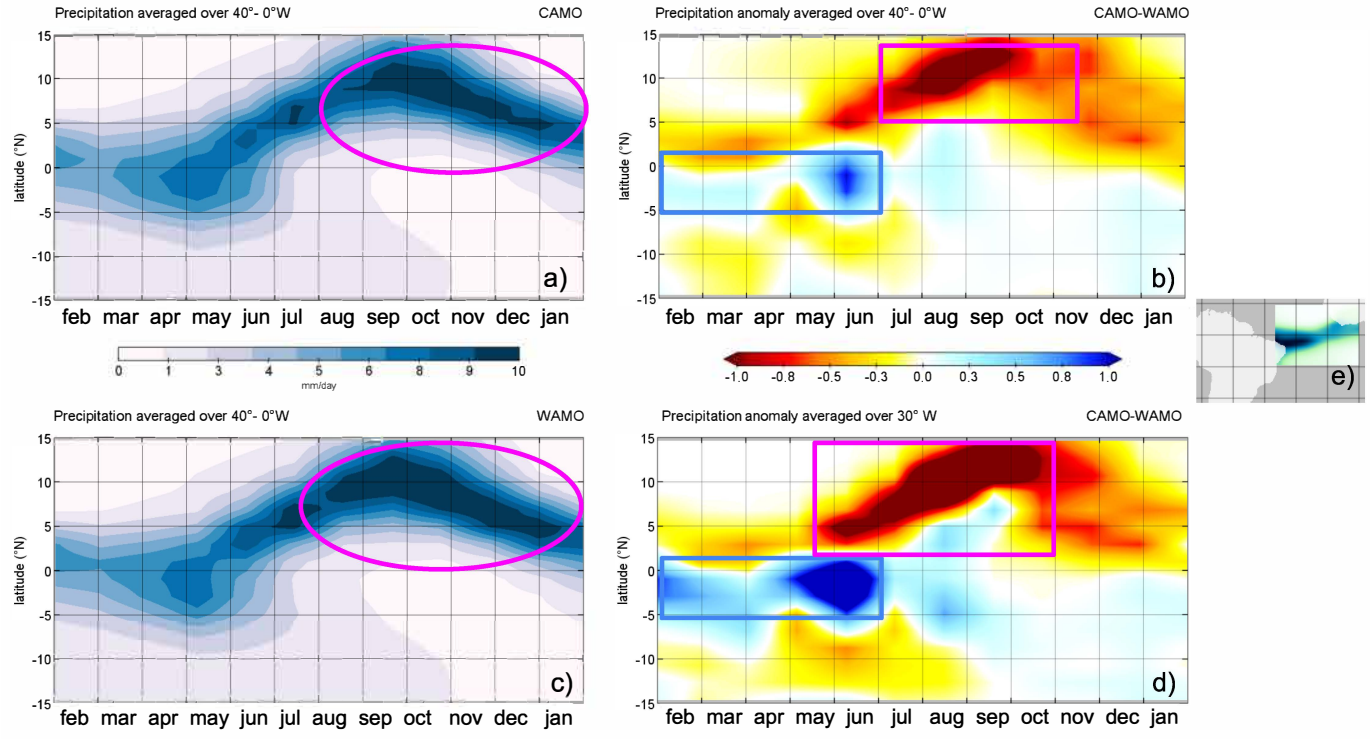

Figure 6. Annual cycle of precipitation for the cold Atlantic Multidecadal Oscillation (CAMO) (**a**) and the warm Atlantic Multidecadal Oscillation (WAMO) (**c**) experiments averaged over 40° W–0°, and their differences averaged over the whole longitudinal band (**b**) of the Atlantic Intertropical Convergence Zone (ITCZ) section (**e**) (15° N–15° S; 40° W–0°) and only at 30° W (**d**), where the precipitation anomaly was the highest.

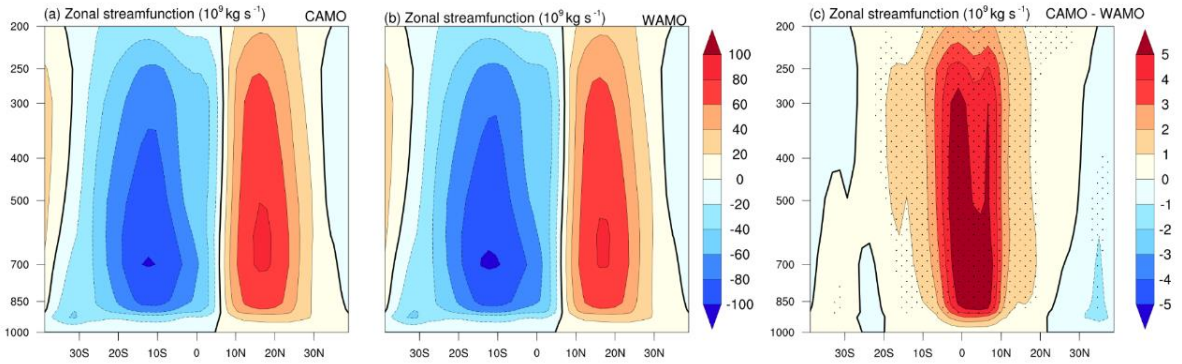

Figure 7. Climatological Hadley cell defined as the zonal mean stream function ψ (10^9 kg/s) for (**a**) CAMO, (**b**) WAMO and the differences between them (**c**). Red and blue contours (solid and dashed lines) denote clockwise and anti-clockwise mass stream functions. Black lines represent the zero-contour stream function. Stippled areas in (**c**) represent statistically significant (Student's *t* test at 95%) differences.

For the vertical profile that represents the Hadley and Walker cells, it is noteworthy that both CAMO and WAMO experiments had the same spatial structure as that of the CONTROL run (Figure S2 and Figure S3 in the Supplementary Materials).

We also looked at the ascending branch of the section of the Atlantic Hadley cell that is situated between the 5° N and 15° S and favors convective activity over this region (Figure 8). The difference (CAMO–WAMO) in vertical velocity at the pressure coordinates shows a dipole of negative/positive values south/north of the equator. This dipole is present in all seasons, with the highest positive anomalies being centered at 4° N in MAM,

indicating a stronger inter-hemispheric atmospheric circulation. In Figure 8, positive anomalies can also be observed north of the equator, which are more pronounced in MAM.

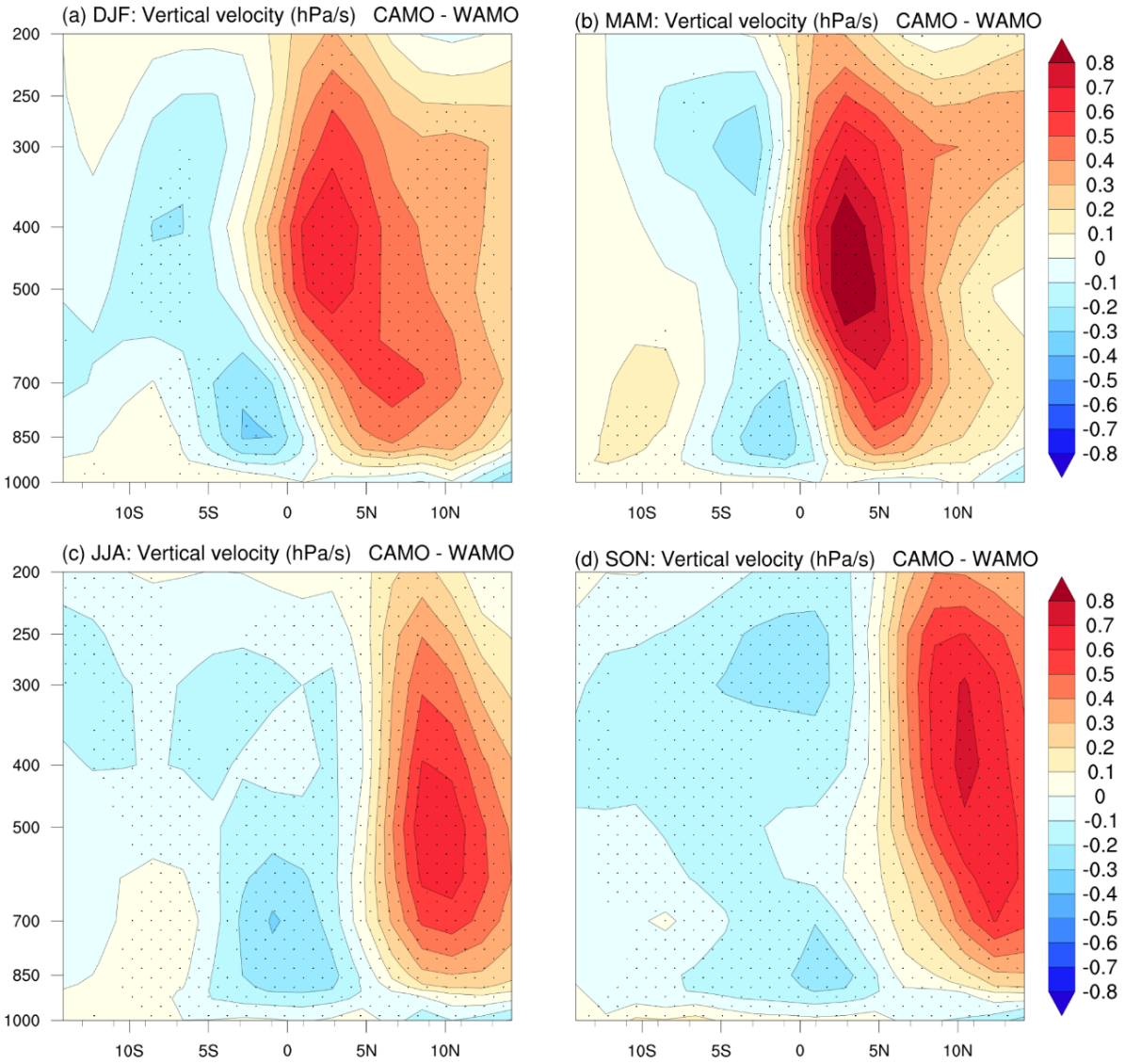

Figure 8. Difference between CAMO and WAMO of vertical pressure velocity (omega; hPa/s) representing the regional Hadley circulation: the latitude–height Section 15° N–15° S, zonally averaged over 80° W–30° W, for (**a**) December–February (DJF), (**b**) March–May (MAM), (**c**) June–August (JJA), and (**d**) September–November (SON). Stippled areas represent statistically significant (Student's *t* test at 95%) differences.

Simultaneously, we find changes in Walker circulation in which the ascending branch is situated right over Amazonia, between the longitudes 80° W–40° W, and the descending motion occurs over longitudes 40° W–20° W (Figure S2 and Figure S3 in the Supplementary Materials). During the cold AMO phase, the ascending motion intensifies (Figure 9a,b). In the DJF and MAM seasons, this negative anomaly has distinct positive anomalies east and west of it, also suggesting a change in the ascending branch position. In SON, the opposite is observed (i.e., significant weakening of the ascending branch).

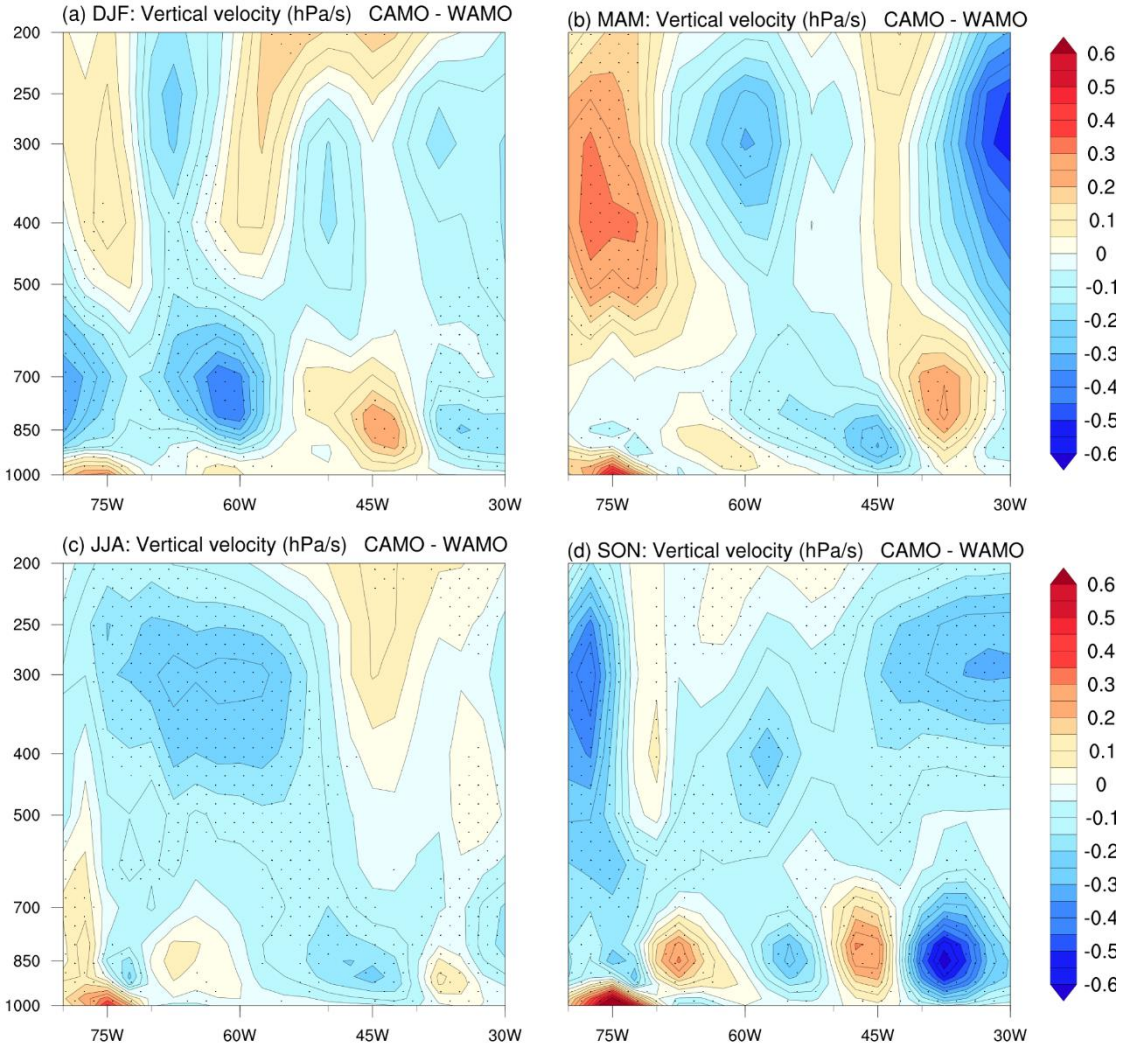

Figure 9. Difference between CAMO and WAMO of vertical pressure velocity (omega; hPa/s) meridionally averaged over 0°–15°S, representing the regional Walker circulation for (**a**) December–February (DJF), (**b**) March–May (MAM), (**c**) June–August (JJA), and (**d**) September–November (SON). Stippled areas represent statistically significant (Student's *t* test at 95%) differences.

4. Discussion

In this section, we explore the mechanisms by which the AMO influences regional precipitation patterns over South America. Our idealized simulations show the AMO as an important driver of changes in precipitation over tropical South America. Mean annual precipitation anomalies undergo a significant reduction over the northern equatorial Atlantic and in most regions of northern South America, as well as a significant increase in the Amazon and northeastern Brazil during the cold AMO phase (Figure 2). Although mean annual precipitation differences are generally consistent with the findings of previous studies [8,16,48] we show that the spatial patterns of precipitation vary seasonally.

Amazonian precipitation changes in our simulations are in agreement with those shown by Yoon and Zeng [48] The authors observed that warming (cooling) of the North Atlantic induced dry (wet) conditions over the Amazon basin. Our results also corroborate their observation that the North Atlantic influence becomes significant over the southern edge of the Amazon basin during the dry season (JJA and SON). These precipitation changes are related to the weakening of SALLJ in JJA and SON, thus reducing the moisture flow from the Amazon to southeastern South America in the cold AMO phase. This differs from the findings presented in Jones and Carvalho [18] (2018). More detailed

analysis is necessary to determine the influence of AMO on SALLJ changes. On the other hand, the results suggest an association between AMO and the Choco low-level jet (CJ) and Caribbean low-level jet (CLLJ) intensity. Our results provide further support for the hypothesis of Loaiza Cerón et al. (2020) [19] that in the cold (warm) AMO phase, CJ is weakened (intensified) and CLLJ is intensified (weakened) (Figure 4d).

For northeastern Brazil, previous studies [8,16] found an increased (decreased) precipitation induced by cold (warm) AMO in the wet season (MAM). In contrast, our model simulation showed an increase in precipitation over northernmost northeastern Brazil and over the adjacent tropical South Atlantic during the CAMO (WAMO) phase, but no clear wet (dry) signal over northeastern Brazil (Figure 2e). There are several possible explanations for these contradictory results: (1) the differences in experimental design and inexistence of feedback between different components which are present in the climate system and in fully coupled models; (2) the complexity of the climate system where the SST variation is not the only or the most important forcing; (3) additional multidecadal influences from SSTs outside the Atlantic [49] or combined impacts of other teleconnection patterns [50,51].

Our results indicate that precipitation anomalies over South America during AMO phases are mainly related to changes in the Hadley cell and subordinately to changes in the Walker cell (Figures 7–9). We find in particular that the global Hadley circulation was strengthened in the NH and weakened in the SH in a cold AMO phase (Table 2). This corroborates previous studies that showed extratropical climate change as an important factor in modulation of Hadley and Walker circulation [52,53]. In addition, our findings are consistent with those of Liu et al. (2020) [54], who identified the multidecadal variability in the strength of the hemispheric Hadley circulation, where intensification in one hemisphere happens together with weakening in the other, resulting in an interhemispheric seesaw in Hadley circulation strength as a response to AMO signal.

We also tested the hypothesis that the AMO phases force the ITCZ to shift meridionally, impacting precipitation over South America, as suggested by previous studies [8,55]. Recently, it was suggested that the ITCZ expansion/contraction may also drive tropical precipitation changes, potentially explaining diverging records [56–60]. To gain further insights, we focus on the position and strength of the Atlantic ITCZ. For the Atlantic ITCZ position, our results do not show a robust meridional shift of ITCZ. The zonal mean precipitation for both AMO phases did not present significant differences in the position of the maximum precipitation (Figure 6). On the other hand, our simulations show significant differences in the Atlantic ITCZ strength, which are evidenced by the positive (negative) precipitation anomalies (CAMO minus WAMO) to the south (north) of the equator. Moreover, the equator-symmetric changes present in precipitation fields are in remarkable agreement with the changes shown in Knight et al. [8].

Atlantic ITCZ strength changes are associated with the Atlantic Hadley cell anomalies (Figure 8), with persistent negative vertical velocity anomalies in the low and middle tropospheric levels between 15° N and 5° S in all seasons during the cold AMO phases. Simultaneously, we find strengthening and eastward shifting of the Walker cell, with the difference being the most pronounced in DJF and MAM.

Our analyses also suggest that the ITCZ response to the AMO is regionally and seasonally dependent. Thus, these responses could be masked in analyses focusing on zonal and annual mean ITCZ shifts, as shown in Mamalakis et al. [61]. Precipitation anomalies (Figure 6b,d) suggest that the core region of ITCZ strengthens (weakens) from February to July, while from July to November the core region weakens (strengthens) during the cold (warm) AMO. This reduction in precipitation over the ITCZ in the winter season during cold AMO is in accordance with the report of Jones and Carvalho [18]. Likewise, Zhou et al. [62] showed that decadal SST variability drives changes in Pacific ITCZ width, highlighting distinct ITCZ changes at seasonal and annual mean timescales.

A recent reconstruction of surface seawater stable oxygen isotopes from the western tropical South Atlantic impacted by the ITCZ, a parameter that is related to changes in

sea surface salinity, indicates a freshening trend from the 1940s to the 1970s (but mainly comprised between the 1960s and the 1970s). The freshening trend was attributed by the authors to a change in the ITCZ [63]. This change would be synchronous with the transition from the warm to the cold AMO (Figure 1), agreeing with our simulations (Figure 2e). However, instead of a southward migration of the ITCZ [63]), we suggest that the observed decline in sea surface salinity in the western tropical South Atlantic was produced by a strengthening of the ITCZ during the cold AMO phase from February to July (Figure 6).

Our results are also in line with those of Roldán-Gómez et al. [64], who showed that ITCZ shifts in the Atlantic during the last millennium were only subordinately impacted by internal variability, and were mainly driven by external forcing. As the results of our study suggest, ITCZ expansion/contraction or changes in its strength are sufficient to produce observed AMO related signals even in the absence of marked changes in the ITCZ position. This implies that ITCZ shifts driven by external forcings (like the large number of strong volcanic eruptions during the Little Ice Age [65] and AMO-induced ITCZ expansion/contraction contribute jointly to changes in precipitation over South America during the last millennium [24,25].

5. Conclusions

We analyzed the dynamical processes involved in South American precipitation changes in response to AMO phases. Unlike most earlier studies that suggest a displacement of the ITCZ, our results do not show robust changes in its zonal mean position between the different AMO phases. Our results suggest that during the cold AMO phase, the NH Hadley circulation was stronger, while the SH Hadley circulation was weaker, which is in agreement with an interhemispheric seesaw in Hadley circulation strength. We also find that the section of the Atlantic Hadley cell is marked by a stronger upward air component south of the equator during the cold AMO phase, which is consistent with distinct positive precipitation anomalies simulated from February to July south of the equator under the Atlantic ITCZ. We interpret the simulated precipitation anomalies as changes in the Atlantic ITCZ core strength, where in the cold (warm) AMO phase the core region of the ITCZ strengthens (weakens) from February to July, while from July to November, the core region weakens (strengthens). It is interesting to note that the Atlantic ITCZ core region is seasonally dependent, such that it is located in the NH most months of the year, except during austral autumn, when it is in the SH [66]. Although the Atlantic ITCZ has a seasonal asymmetry, the AMO has a nearly symmetric effect in modulating the Atlantic ITCZ-related precipitation. We also find that during the cold AMO phase the ascending branch of the Walker circulation placed over western Amazonia is intensified and shifted eastward.

Our results stress the importance of acknowledging the dynamics of season- and regional-dependent ITCZ responses as they are sufficient to produce observed AMO-related signals even in the absence of marked changes in the ITCZ position. In addition, our results provide a better understanding of the physical basis of the AMO-related changes in South American precipitation. This understanding will serve as a base for the exploration of simulated water isotopes, with the aim to investigate the isotopic fingerprint of AMO and precipitation variability found in paleoclimate reconstructions over South America.

Supplementary Materials: The following supporting information can be downloaded at: https://www.mdpi.com/article/10.3390/atmos13111778/s1.

Author Contributions: Conceptualization—J.M., M.H.S. and M.P.; Methodology—J.M., M.H.S. and M.P.; Software was managed by J.M., M.H.S.; Validation—J.M., M.H.S., G.S. and M.P.; Formal analysis—J.M., M.H.S., G.S. and M.P.; Investigation—J.M., M.H.S.; Data curation—J.M., M.H.S. Original draft preparation—J.M.; Reviewing and editing—J.M., M.H.S., G.S, M.T.K., C.M.C. and M.P.; Visualization—J.M., M.H.S.; Supervision—G.S. All authors have read and agreed to the published version of the manuscript.

Funding: Maksic acknowledges the financial support from FAPESP (grant 2018/23522-6). C.M. Chiessi acknowledges the financial support from FAPESP (grants 2018/15123-4 and 2019/24349-9) and CNPq (grant 312458/2020-7).

Conflicts of Interest: The authors declare no conflict of interest. The founding sponsors had no role in the design, analysis and interpretation of data, in the writing manuscript, or in the decision to publish the results.

References

1. Folland, C.K.; Parker, D.E.; Kates, F.E. Worldwide marine temperature fluctuations 1856–1981. *Nature* **1984**, *310*, 670–673. [CrossRef]
2. Enfield, D.B.; Mestas-Nuñez, A.M.; Trimble, P.J. The Atlantic multidecadal oscillation and its relation to rainfall and river flows in the continental US. *Geophys. Res. Lett.* **2001**, *28*, 2077–2080. [CrossRef]
3. Trenberth, K.E.; Shea, D.J. Atlantic hurricanes and natural variability in 2005. *Geophys. Res. Lett.* **2006**, *33*. [CrossRef]
4. Guan, B.; Nigam, S. Analysis of Atlantic SST Variability Factoring Interbasin Links and the Secular Trend: Clarified Structure of the Atlantic Multidecadal Oscillation. *J. Clim.* **2009**, *22*, 4228–4240. [CrossRef]
5. Knight, J.R. The Atlantic Multidecadal Oscillation Inferred from the Forced Climate Response in Coupled General Circulation Models. *J. Clim.* **2009**, *22*, 1610–1625. [CrossRef]
6. Ting, M.; Kushnir, Y.; Seager, R.; Li, C. Forced and Internal Twentieth-Century SST Trends in the North Atlantic*. *J. Clim.* **2009**, *22*, 1469–1481. [CrossRef]
7. Schlesinger, M.E.; Ramankutty, N. An oscillation in the global climate system of period 65–70 years. *Nature* **1994**, *367*, 723–726. [CrossRef]
8. Knight, J.R.; Folland, C.K.; Scaife, A.A. Climate impacts of the Atlantic Multidecadal Oscillation. *Geophys. Res. Lett.* **2006**, *33*. [CrossRef]
9. Zhang, R.; Delworth, T.L. Impact of Atlantic multidecadal oscillations on India/Sahel rainfall and Atlantic hurricanes. *Geophys. Res. Lett.* **2006**, *33*. [CrossRef]
10. Sutton, R.T.; Hodson, D.L.R. Atlantic Ocean Forcing of North American and European Summer Climate. *Science* **2005**, *309*, 115–118. [CrossRef]
11. Wang, C.; Dong, S.; Evan, A.T.; Foltz, G.; Lee, S.-K. Multidecadal Covariability of North Atlantic Sea Surface Temperature, African Dust, Sahel Rainfall, and Atlantic Hurricanes. *J. Clim.* **2012**, *25*, 5404–5415. [CrossRef]
12. Lu, R.; Dong, B.; Ding, H. Impact of the Atlantic Multidecadal Oscillation on the Asian summer monsoon. *Geophys. Res. Lett.* **2006**, *33*. [CrossRef]
13. Wang, Y.; Li, S.; Luo, D. Seasonal response of Asian monsoonal climate to the Atlantic Multidecadal Oscillation. *J. Geophys. Res. Earth Surf.* **2009**, *114*. [CrossRef]
14. Miao, J.; Jiang, D. Multidecadal Variations in the East Asian Winter Monsoon and Their Relationship with the Atlantic Multidecadal Oscillation since 1850. *J. Clim.* **2021**, *34*, 7525–7539. [CrossRef]
15. Krishnamurthy, L.; Krishnamurthy, V. Teleconnections of Indian monsoon rainfall with AMO and Atlantic tripole. *Clim. Dyn.* **2015**, *46*, 2269–2285. [CrossRef]
16. Kayano, M.T.; Capistrano, V.B.; Andreoli, R.V.; de Souza, R.A.F. A further analysis of the tropical Atlantic SST modes and their relations to north-eastern Brazil rainfall during different phases of Atlantic Multidecadal Oscillation. *Int. J. Clim.* **2016**, *36*, 4006–4018. [CrossRef]
17. Kayano, M.T.; Setzer, A.W. Nearly Synchronous Multidecadal Oscillations of Surface Air Temperature in Punta Arenas and the Atlantic Multidecadal Oscillation Index. *J. Clim.* **2018**, *31*, 7237–7248. [CrossRef]
18. Jones, C.; Carvalho, L.M.V. The influence of the Atlantic multidecadal oscillation on the eastern Andes low-level jet and precipitation in South America. *npj Clim. Atmos. Sci.* **2018**, *1*, 40. [CrossRef]
19. Cerón, W.L.; Andreoli, R.V.; Kayano, M.T.; de Souza, R.A.F.; Jones, C.; Carvalho, L.M.V. The Influence of the Atlantic Multidecadal Oscillation on the Choco Low-Level Jet and Precipitation in Colombia. *Atmosphere* **2020**, *11*, 174. [CrossRef]
20. Saenger, C.; Cohen, A.L.; Oppo, D.W.; Halley, R.B.; Carilli, J.E. Surface-temperature trends and variability in the low-latitude North Atlantic since 1552. *Nat. Geosci.* **2009**, *2*, 492–495. [CrossRef]
21. Zhang, R.; Sutton, R.; Danabasoglu, G.; Kwon, Y.; Marsh, R.; Yeager, S.G.; Amrhein, D.E.; Little, C.M. A Review of the Role of the Atlantic Meridional Overturning Circulation in Atlantic Multidecadal Variability and Associated Climate Impacts. *Rev. Geophys.* **2019**, *57*, 316–375. [CrossRef]
22. Chiessi, C.M.; Mulitza, S.; Pätzold, J.; Wefer, G.; Marengo, J.A. Possible impact of the Atlantic Multidecadal Oscillation on the South American summer monsoon. *Geophys. Res. Lett.* **2009**, *36*. [CrossRef]
23. Bernal, J.; Cruz, F.W.; Stríkis, N.M.; Wang, X.; Deininger, M.; Catunda, M.C.A.; Ortega-Obregón, C.; Cheng, H.; Edwards, R.L.; Auler, A.S. High-resolution Holocene South American monsoon history recorded by a speleothem from Botuverá Cave, Brazil. *Earth Planet. Sci. Lett.* **2016**, *450*, 186–196. [CrossRef]

24. Apaéstegui, J.; Cruz, F.W.; Sifeddine, A.; Vuille, M.; Espinoza, J.C.; Guyot, J.L.; Khodri, M.; Strikis, N.; Santos, R.V.; Cheng, H.; et al. Hydroclimate variability of the northwestern Amazon Basin near the Andean foothills of Peru related to the South American Monsoon System during the last 1600 years. *Clim. Past* **2014**, *10*, 1967–1981. [CrossRef]
25. Novello, V.F.; Cruz, F.W.; Moquet, J.S.; Vuille, M.; de Paula, M.S.; Nunes, D.; Edwards, R.L.; Cheng, H.; Karmann, I.; Utida, G.; et al. Two Millennia of South Atlantic Convergence Zone Variability Reconstructed From Isotopic Proxies. *Geophys. Res. Lett.* **2018**, *45*, 5045–5051. [CrossRef]
26. Garcia, S.R.; Kayano, M.T. Some evidence on the relationship between the South American monsoon and the Atlantic ITCZ. *Arch. Meteorol. Geophys. Bioclimatol. Ser. B* **2009**, *99*, 29–38. [CrossRef]
27. Garreaud, R.; Vuille, M.; Compagnucci, R.; Marengo, J. Present-day South American climate. *Palaeogeogr. Palaeoclim. Palaeoecol.* **2009**, *281*, 180–195. [CrossRef]
28. Meehl, G.A.; Covey, C.; Delworth, T.; Latif, M.; McAvaney, B.; Mitchell, J.F.B.; Stouffer, R.J.; Taylor, K.E. THE WCRP CMIP3 Multimodel Dataset: A New Era in Climate Change Research. *Bull. Am. Meteorol. Soc.* **2007**, *88*, 1383–1394. [CrossRef]
29. Taylor, K.E.; Stouffer, R.J.; Meehl, G.A. An Overview of CMIP5 and the Experiment Design. *Bull. Am. Meteorol. Soc.* **2012**, *93*, 485–498. [CrossRef]
30. Eyring, V.; Bony, S.; Meehl, G.A.; Senior, C.A.; Stevens, B.; Stouffer, R.J.; Taylor, K.E. Overview of the Coupled Model Intercomparison Project Phase 6 (CMIP6) experimental design and organization. *Geosci. Model. Dev.* **2016**, *9*, 1937–1958. [CrossRef]
31. Murphy, L.N.; Bellomo, K.; Cane, M.; Clement, A. The role of historical forcings in simulating the observed Atlantic multidecadal oscillation. *Geophys. Res. Lett.* **2017**, *44*, 2472–2480. [CrossRef]
32. Han, Z.; Luo, F.; Li, S.; Gao, Y.; Furevik, T.; Svendsen, L. Simulation by CMIP5 models of the atlantic multidecadal oscillation and its climate impacts. *Adv. Atmos. Sci.* **2016**, *33*, 1329–1342. [CrossRef]
33. Ruiz-Barradas, A.; Nigam, S.; Kavvada, A. The Atlantic Multidecadal Oscillation in twentieth century climate simulations: Uneven progress from CMIP3 to CMIP5. *Clim. Dyn.* **2013**, *41*, 3301–3315. [CrossRef]
34. Koster, R.D.; Dirmeyer, P.A.; Guo, Z.; Bonan, G.; Chan, E.; Cox, P.; Gordon, C.T.; Kanae, S.; Kowalczyk, E.; Lawrence, D.; et al. Regions of Strong Coupling Between Soil Moisture and Precipitation. *Science* **2004**, *305*, 1138–1140. [CrossRef] [PubMed]
35. Mueller, B.; Seneviratne, S.I. Systematic land climate and evapotranspiration biases in CMIP5 simulations. *Geophys. Res. Lett.* **2013**, *41*, 128–134. [CrossRef] [PubMed]
36. Mystakidis, S.; Seneviratne, S.I.; Gruber, N.; Davin, E.L. Hydrological and biogeochemical constraints on terrestrial carbon cycle feedbacks. *Environ. Res. Lett.* **2017**, *12*, 014009. [CrossRef]
37. Hawcroft, M.; Haywood, J.M.; Collins, M.; Jones, A.; Jones, A.C.; Stephens, G. Southern Ocean albedo, inter-hemispheric energy transports and the double ITCZ: Global impacts of biases in a coupled model. *Clim. Dyn.* **2016**, *48*, 2279–2295. [CrossRef]
38. Hodson, D.L.R.; Bretonnière, P.-A.; Cassou, C.; Davini, P.; Klingaman, N.P.; Lohmann, K.; Lopez-Parages, J.; Martín-Rey, M.; Moine, M.-P.; Monerie, P.-A.; et al. Coupled climate response to Atlantic Multidecadal Variability in a multi-model multi-resolution ensemble. *Clim. Dyn.* **2022**, *59*, 805–836. [CrossRef]
39. Brady, E.; Stevenson, S.; Bailey, D.; Liu, Z.; Noone, D.; Nusbaumer, J.; Otto-Bliesner, B.L.; Tabor, C.; Tomas, R.; Wong, T.; et al. The Connected Isotopic Water Cycle in the Community Earth System Model Version 1. *J. Adv. Model. Earth Syst.* **2019**, *11*, 2547–2566. [CrossRef]
40. Stevenson, S.; Otto-Bliesner, B.L.; Brady, E.C.; Nusbaumer, J.; Tabor, C.; Tomas, R.; Noone, D.C.; Liu, Z. Volcanic Eruption Signatures in the Isotope-Enabled Last Millennium Ensemble. *Paleoceanogr. Paleoclimatol.* **2019**, *34*, 1534–1552. [CrossRef]
41. Nusbaumer, J.; Wong, T.E.; Bardeen, C.; Noone, D. Evaluating hydrological processes in the Community Atmosphere Model Version 5 (C AM5) using stable isotope ratios of water. *J. Adv. Model. Earth Syst.* **2017**, *9*, 949–977. [CrossRef]
42. Neale, R.B.; Chen, C.C.; Gettelman, A.; Lauritzen, P.H.; Park, S.; Williamson, D.L.; Conley, A.J.; Garcia, R.; Kinnison, D.; Lamarque, J.F.; et al. Description of the NCAR Community Atmosphere Model (CAM 5.0) (No. NCAR/TN-486+ STR). *NCAR Tech.* **2010**, *1*, 1–12.
43. Oleson, K.W.; Lawrence, D.M.; Gordon, B.; Flanner, M.G.; Kluzek, E.; Peter, J.; Levis, S.; Swenson, S.C.; Thornton, E.; Feddema, J.; et al. *Technical Description of Version 4.0 of the Community Land Model (CLM)*; UCAR: Boulder, CO, USA, 2010.
44. Rayner, N.A.; Brohan, P.; Parker, D.E.; Folland, C.K.; Kennedy, J.J.; Vanicek, M.; Ansell, T.J.; Tett, S.F.B. Improved analyses of changes and uncertainties in sea surface temperature measured in situ since the mid-nineteenth century: The HadSST2 data set. *J. Clim.* **2006**, *19*, 446–469. [CrossRef]
45. Slivinski, L.C.; Compo, G.P.; Whitaker, J.S.; Sardeshmukh, P.D.; Giese, B.S.; McColl, C.; Allan, R.; Yin, X.; Vose, R.; Titchner, H.; et al. Towards a more reliable historical reanalysis: Improvements for version 3 of the Twentieth Century Reanalysis system. *Q. J. R. Meteorol. Soc.* **2019**, *145*, 2876–2908. [CrossRef]
46. Nguyen, H.; Evans, A.; Lucas, C.; Smith, I.; Timbal, B. The Hadley Circulation in Reanalyses: Climatology, Variability, and Change. *J. Clim.* **2013**, *26*, 3357–3376. [CrossRef]
47. Levine, A.F.Z.; Frierson, D.M.W.; McPhaden, M.J. AMO Forcing of Multidecadal Pacific ITCZ Variability. *J. Clim.* **2018**, *31*, 5749–5764. [CrossRef]
48. Yoon, J.-H.; Zeng, N. An Atlantic influence on Amazon rainfall. *Clim. Dyn.* **2009**, *34*, 249–264. [CrossRef]
49. Cerón, W.L.; Kayano, M.T.; Andreoli, R.V.; Avila-Diaz, A.; de Souza, I.P.; Souza, R.A.F. Pacific and Atlantic Multidecadal Variability Relations with the Choco and Caribbean Low-Level Jets during the 1900–2015 Period. *Atmosphere* **2021**, *12*, 1120. [CrossRef]

50. Reboita, M.S.; Ambrizzi, T.; Crespo, N.M.; Dutra, L.M.M.; Ferreira, G.W.d.S.; Rehbein, A.; Drumond, A.; da Rocha, R.P.; de Souza, C.A. Impacts of teleconnection patterns on South America climate. *Ann. N. Y. Acad. Sci.* **2021**, *1504*, 116–153. [CrossRef]
51. Kayano, M.T.; Cerón, W.L.; Andreoli, R.V.; Souza, R.A.; Avila-Diaz, A.; Zuluaga, C.F.; Carvalho, L.M. Does the El Niño-Southern Oscillation Affect the Combined Impact of the Atlantic Multidecadal Oscillation and Pacific Decadal Oscillation on the Precipitation and Surface Air Temperature Variability over South America? *Atmosphere* **2022**, *13*, 231. [CrossRef]
52. Frierson, D.M.W.; Hwang, Y.-T. Extratropical Influence on ITCZ Shifts in Slab Ocean Simulations of Global Warming. *J. Clim.* **2012**, *25*, 720–733. [CrossRef]
53. Kang, S.M.; Xie, S.-P.; Shin, Y.; Kim, H.; Hwang, Y.-T.; Stuecker, M.F.; Xiang, B.; Hawcroft, M. Walker circulation response to extratropical radiative forcing. *Sci. Adv.* **2020**, *6*, eabd3021. [CrossRef] [PubMed]
54. Liu, Y.; Gong, Z.; Sun, C.; Li, J.; Wang, L. Multidecadal Seesaw in Hadley Circulation Strength Between the Two Hemispheres Caused by the Atlantic Multidecadal Variability. *Front. Earth Sci.* **2020**, *8*. [CrossRef]
55. Ting, M.; Kushnir, Y.; Seager, R.; Li, C. Robust features of Atlantic multi-decadal variability and its climate impacts. *Geophys. Res. Lett.* **2011**, *38*. [CrossRef]
56. Yan, H.; Wei, W.; Soon, W.; An, Z.; Zhou, W.; Liu, Z.; Wang, Y.; Carter, R.M. Dynamics of the intertropical convergence zone over the western Pacific during the Little Ice Age. *Nat. Geosci.* **2015**, *8*, 315–320. [CrossRef]
57. Wodzicki, K.R.; Rapp, A.D. Long-term characterization of the Pacific ITCZ using TRMM, GPCP, and ERA-Interim. *J. Geophys. Res. Atmos.* **2016**, *121*, 3153–3170. [CrossRef]
58. Utida, G.; Cruz, F.; Etourneau, J.; Bouloubassi, I.; Schefuß, E.; Vuille, M.; Novello, V.F.; Prado, L.; Sifeddine, A.; Klein, V.; et al. Tropical South Atlantic influence on Northeastern Brazil precipitation and ITCZ displacement during the past 2300 years. *Sci. Rep.* **2019**, *9*, 1–8. [CrossRef]
59. Asmerom, Y.; Baldini, J.U.L.; Prufer, K.M.; Polyak, V.J.; Ridley, H.E.; Aquino, V.V.; Baldini, L.M.; Breitenbach, S.F.M.; Macpherson, C.G.; Kennett, D.J. Intertropical convergence zone variability in the Neotropics during the Common Era. *Sci. Adv.* **2020**, *6*, eaax3644. [CrossRef]
60. Chiessi, C.M.; Mulitza, S.; Taniguchi, N.K.; Prange, M.; Campos, M.C.; Häggi, C.; Schefuß, E.; Pinho, T.M.L.; Frederichs, T.; Portilho-Ramos, R.C.; et al. Mid- to Late Holocene Contraction of the Intertropical Convergence Zone Over Northeastern South America. *Paleoceanogr. Paleoclimatol.* **2021**, *36*. [CrossRef]
61. Mamalakis, A.; Randerson, J.T.; Yu, J.-Y.; Pritchard, M.S.; Magnusdottir, G.; Smyth, P.; Levine, P.A.; Yu, S.; Foufoula-Georgiou, E. Zonally contrasting shifts of the tropical rain belt in response to climate change. *Nat. Clim. Chang.* **2021**, *11*, 143–151. [CrossRef] [PubMed]
62. Zhou, W.; Leung, L.R.; Lu, J.; Yang, D.; Song, F. Contrasting Recent and Future ITCZ Changes From Distinct Tropical Warming Patterns. *Geophys. Res. Lett.* **2020**, *47*. [CrossRef]
63. Pereira, N.; Clarke, L.; Chiessi, C.; Kilbourne, K.; Crivellari, S.; Cruz, F.; Campos, J.; Yu, T.-L.; Shen, C.-C.; Kikuchi, R.; et al. Mid to late 20th century freshening of the western tropical South Atlantic triggered by southward migration of the Intertropical Convergence Zone. *Palaeogeogr. Palaeoclim. Palaeoecol.* **2022**, *597*, 111013. [CrossRef]
64. Roldán-Gómez, P.J.; González-Rouco, J.F.; Melo-Aguilar, C.; Smerdon, J.E. The Role of Internal Variability in ITCZ Changes Over the Last Millennium. *Geophys. Res. Lett.* **2022**, *49*. [CrossRef]
65. Tejedor, E.; Steiger, N.J.; Smerdon, J.E.; Serrano-Notivoli, R.; Vuille, M. Global hydroclimatic response to tropical volcanic eruptions over the last millennium. *Proc. Natl. Acad. Sci. USA* **2021**, *118*. [CrossRef] [PubMed]
66. Chiang, J.C.H.; Kushnir, Y.; Giannini, A. Deconstructing Atlantic Intertropical Convergence Zone variability: Influence of the local cross-equatorial sea surface temperature gradient and remote forcing from the eastern equatorial Pacific. *J. Geophys. Res. Earth Surf.* **2002**, *107*, ACL 3-1–ACL 3-19. [CrossRef]